

Spatiotemporal bursting in simulated cultures of cortical neurons

Michael Stiber^{a,*}, Natalie Gonzales^a, Jewel YunHsuan Lee^b

^a *University of Washington Bothell, Computing and Software Systems Division, Box 358534, 18115 Campus Way NE, Bothell, WA, 98011, USA*

^b *Ultrasound R&D, Philips Healthcare, 22100 Bothell Everett Hwy, Bothell, WA, 98021, USA*

Abstract

Cultures of neurons grown on multi-electrode arrays have become a common experimental preparation for investigating developing neural networks. Experiment and simulation have shown that these developing networks eventually exhibit bursting behavior in which the entire culture participates for short periods of time, with inter-burst intervals in which the network is comparatively quiescent. This paper extends previous simulation results by examining the spatiotemporal patterns of such bursting. We show that these bursts originate at a small number of network locations and propagate as waves of activity. We demonstrate that this type of activity does not require fine tuning of neuron or network parameters. We also examine how this activity changes during development and the dependence of such activity and its triggering on both local and global network properties.

Keywords: Spiking Activity, Burst Detection, Burst initiation, Spatiotemporal Data Analysis, Bursting, Simulation

1. Introduction

Neural circuits are nonlinear systems that produce an immense range of complex behaviors. These circuits are composed of individual cells, whose molecular and dynamical activities govern development of network connectivity and give rise to an organism's sensory processing, motor activity, and behavior (not to mention such phenomena as consciousness). The relationships among these multiple spatiotemporal levels of detail are complex, and the basic principles of how individual neurons' activities produce development and computation in networks is still largely unknown. One approach to examining this question has

*Corresponding author

Email addresses: stiber@uw.edu (Michael Stiber), ngonza5@uw.edu (Natalie Gonzales), jewel.yh.lee@gmail.com (Jewel YunHsuan Lee)

URL: faculty.washington.edu/stiber (Michael Stiber)

been to study cultures of mammalian cortical neurons as they form functioning networks on multi-electrode arrays (MEAs) (Thomas et al., 1972; Gross, 1979; Pine, 1980). These cultures allow stimulation and recording from individual cells, or local groups of cells, over time as networks develop. As such, they can serve as platforms for investigating the interplay among individual neuron dynamics, network development, and network dynamics.

One of the major features of network dynamics in such cultures is a convergence to whole-culture bursting (Maeda et al., 1995; vanPelt et al., 2004; Stegenga et al., 2008; Gritsun et al., 2012). This is a type of spontaneous activity in which most or all neurons in the culture participate in synchronized spiking over a brief period of time. These bursts begin to occur during network development, repeating at irregular intervals and developing increased intensity and decreased duration.

Maeda et al. (1995) demonstrated that these bursts originate in small regions of the network and propagate directionally across it. This was later confirmed in extensive experimental results in which the originating sets of neurons were termed *leaders* (Eytan and Marom, 2006; Eckmann et al., 2008; Pasquale et al., 2013; Lonardonni et al., 2017; Pasquale et al., 2017). Moreover, these bursts were shown early on to propagate directionally across networks (Maeda et al., 1995); later results have been consistent with the interpretation of this as traveling waves of activity (Sato et al., 2012; Okujeni et al., 2017), which is consistent with observations of traveling waves in mammalian cortex (Muller et al., 2018; Davis et al., 2020, 2021; Klavinskis-Whiting et al., 2023).

Simulations of such networks can exhibit many of the same behaviors. Gritsun et al. (2012) developed a detailed model of neurite outgrowth in such preparations, and used that to produce connectivity patterns that were then incorporated into simulations of network spiking activity; data was collected from a simulated electrode array. These showed whole-network bursting activity, inter-burst timing, and wave-like propagation consistent with those observed in living preparations. However, simpler models can produce similar results; networks of spiking neurons and phase oscillators will produce traveling waves originating at the equivalent of leaders (Ermentrout and Kleinfeld, 2001; Zbinden, 2011; Sakuma et al., 2016; Huang et al., 2017; Paraskevov and Zendrikov, 2017; Senk et al., 2020).

In our own previous work (Kawasaki and Stiber, 2012, 2014), closed-loop, MEA-scale simulations were developed that modeled the entire network developmental period at the temporal resolution of individual neuron spiking behavior. These simulations captured the effect of neural activity on neurite outgrowth, and vice versa, using simple neuron and outgrowth models. Exploration of a set of model parameters showed a broad region of that parameter space that produced stable network bursting behavior. Examination of that behavior showed burst development, burst shape, and inter-burst timing consistent with the living preparations. This demonstrated that these aspects of network dynamics could be substantially captured by closed-loop models with relatively simple dynamics. It also reinforced the conclusion that such network bursting was an emergent behavior that did not require neuron models capable of autonomous

bursting behavior.

This paper presents results from simulations of closed-loop, MEA-scale simulations of development in cortical cultures that exhibit whole-network bursting. It examines the relationship between individual neuron spiking and spatiotemporal network behavior, determining burst spatiotemporal shape, where in the culture bursts originate, how they propagate, and how burst origination changes as network connectivity develops. It accomplishes this by extending our previous work (which had only examined whole-network temporal activity) by capturing the time of each spike produced by each neuron in the simulation.

2. Modeling and Simulation

The overarching goal of this work has been to develop models that include the minimal dynamics at each level that is necessary to reproduce behaviors seen in living systems, and then to simulate these models at the time scale of spike production to capture the time of each spike from every neuron. The key model and simulation features, described in subsequent sections (with parameter values and simulation procedures defined in detail by Kawasaki and Stiber (2014)), are:

- Leaky integrator neuron model.
- Spike-coupled network arranged in a 2D grid.
- Synapses that include dynamics of resource depletion and recovery.
- Simple neuron-activity-dependent network development model that does not include such things as spike-timing-dependent plasticity.
- Simulation of equivalent of 28 days of *in vitro* network development with 0.1ms time step.
- Network behaviors are an emergent property; only two parameters (one for neurite outgrowth and one determining balance of inhibitory and excitatory neurons) are explored to identify region of that parameter space producing stationary bursting.

2.1. Neuron and Synapse Models

These simulations use a lumped, leaky integrator neuron model that includes synaptic, bias, and noise currents (Abbott, 1999):

$$C_m \frac{dV_m}{dt} = \frac{1}{R_m} (V_{\text{rest}} - V_m) + I_{\text{syn}} + I_{\text{inj}} + I_{\text{noise}} \quad (1)$$

with V_{rest} being both the asymptotic and reset potential, I_{syn} the total synaptic current, I_{inj} a constant depolarizing current, I_{noise} a noise current, and C_m and R_m the membrane capacitance and resistance, respectively. When V_m exceeds V_{thresh} , the firing threshold, a spike event is generated and V_m is set to V_{rest} . This model also incorporates an absolute refractory period, T_{refract} . Parameters

are set so that most neurons do not produce spikes in the absence of excitatory input; a subset of cells are selected as endogenously active and have their V_{thresh} reduced so that they will spontaneously fire.

Generated spikes are transmitted to connected neurons after fixed delays via synapses with activity-dependent facilitation and depression (Markram et al., 1998; Tsodyks et al., 1998) with four state variables: three that govern the fraction of synaptic resources in particular states — x (recovered state), y (active state), and z (inactive state) — and one, u , that represents synaptic efficiency:

$$\frac{dx}{dt} = \frac{z}{\tau_{\text{rec}}} - ux\delta(t - t_{\text{sp}}) \quad (2)$$

$$\frac{dy}{dt} = -\frac{y}{\tau_I} + Ux\delta(t - t_{\text{sp}}) \quad (3)$$

$$\frac{dz}{dt} = \frac{y}{\tau_I} - \frac{z}{\tau_{\text{rec}}} \quad (4)$$

$$\frac{du}{dt} = -\frac{u}{\tau_{\text{facil}}} + U(1 - u)\delta(t - t_{\text{sp}}) \quad (5)$$

Here, $\delta(t - t_{\text{sp}})$ is the unit impulse at the arriving spike time t_{sp} . The three time constants τ_I , τ_{rec} , and τ_{facil} govern inactivation after an arriving spike, recovery from inactivation, and facilitation after a spike, respectively. The synaptic current produced by an arriving spike is $I_{\text{syn}} = Wy$, where W is the strength of the connection determined by the development model, described in the next section. Synapse parameters vary according to the combination of presynaptic and postsynaptic neuron type (excitatory or inhibitory) (Kawasaki and Stiber, 2014).

2.2. Development and Network Models

The cortical culture model is composed of a 100×100 array of neurons, arranged in a rectangular grid as a 10×10 pattern of inhibitory, excitatory, and endogenously active cells that is tiled 10 times horizontally and vertically to form the whole network (Kawasaki and Stiber, 2014). Existence and strength, W , of connections between any two neurons is governed by a neurite outgrowth model in which each neuron's set of neurites is modeled as filling a circle centered on that neuron with uniform density. The radius of each neuron's circle of connectivity varies according to (Van Ooyen et al., 1995; Van Ooyen and Van Pelt, 1996):

$$\frac{dR_i}{dt} = \rho G(F_i) \quad (6)$$

$$G(F_i) = 1 - \frac{2}{1 + \exp((\epsilon - F_i)/\beta)} \quad (7)$$

Here, R_i is the radius of neuron i 's circle of connectivity, F_i is neuron i 's recent average firing rate (normalized within the range $[0, 1]$), ρ is a rate constant, ϵ is the outgrowth null point, and β controls the sensitivity of outgrowth to F_i .

Connections are established between neurons that have circles of connectivity that overlap, with W for them proportional to area of overlap, consistent with the simplifying assumption that neurite density is uniform within such circles and thus number of synapses will be proportional to area of overlap.

2.3. Simulation and Data Collection

We used the Graphitti graph-based systems simulator (Stiber et al., 2025a, 2018, 2017) to perform simulations equivalent to 28 days' development for four networks with two different values each for the growth parameter ϵ (1.0 and 1.9) and the network structure parameter governing fraction of cells that were excitatory (90% and 98%). These corresponded to four simulations that previously produced stationary bursting (Kawasaki and Stiber, 2014). These simulations were re-run on an Intel Xeon server running Ubuntu Linux 16.04.3 using an NVIDIA Tesla K80 GPU with CUDA 8.0 libraries. Spike times (and corresponding neuron (x, y) location) were recorded to HDF5 files with 0.1ms resolution, along with spike counts for the entire network within 10ms bins. Binned spike counts for each simulation were compared to previous results (Kawasaki and Stiber, 2014) (in which such counts were also collected) to verify that the new and old simulation results were qualitatively identical (unavoidable differences in noise realizations prevent precise numerical equality).

3. Analysis

Three major categories of data analyses were performed, as described in detail in the following subsections:

1. Whole-network bursts, and their constituent spikes, were identified and their spatiotemporal patterns were visualized.
2. Burst origin locations were determined.
3. Bursts that originated independently near the same time, and that therefore produced overlapping wavefronts, were identified and excluded from further analysis.
4. The speed of propagation of the burst wavefronts was computed and the variation in mean propagation speed during network development was visualized.
5. The sequence of burst origin locations during network development was described and their spatial distribution and sequential correlation were analyzed.
6. The relationship during development between burst origins and endogenously active neuron spiking rate was investigated.

Analyses were performed in Matlab (Stiber et al., 2025b).

3.1. Burst Identification and Visualization

Bursts were identified as in previous work (Kawasaki and Stiber, 2014), using the count of spikes produced by the entire network within 10ms bins (consistent with methods in the physiological literature regarding bursting in cortical cultures). Sequences of bins with spike counts above 50 (corresponding to a spike rate threshold of 0.5 spikes/second/neuron) were considered to be within bursts, with the first bin in a sequence being the burst start and the final bin in a sequence being burst end. Thus, start and end times were determined with 10ms start and end time accuracy. These start and end times were then used to select, for each burst, the set of spikes produced by each neuron that were considered part of the burst. Because there was ongoing background neuronal activity, a very small number of spikes associated with each burst were not causally connected to the bursting behavior itself, but they were insignificantly few compared to the number of spikes in each burst.

These spikes were then used to visualize each burst’s spatiotemporal pattern. Bursts were segmented into 10ms non-overlapping windows and the number of spikes produced by each neuron in the 100×100 network was used to generate an image representing spiking intensity with color (blue to red) indicating spiking rate (zero to highest in that window). These images were either output individually or concatenated to produce videos.

3.2. Burst Origins

Examination of spatiotemporal patterns revealed that each burst initiated within a very small, compact cluster of cells. Each burst b_i initiation was therefore analyzed to assign an (x_i, y_i) *origin* point. The 10ms windows previously described were used for this purpose. Within each burst these windows were scanned to find the first one in which at least three neurons produced at least two spikes. This was done to separate the clear start of bursting from background activity and also to take into account that there was a very small probability (from the current data, less than one in 5000) that multiple bursts might originate close in time. Within that window, those neurons that produced the most spikes were identified as the set of most active cells. To guard against multiple bursts (and therefore multiple clusters), each neuron was examined, and removed from that set if the subset of neurons it was close to was smaller than the subset that it was far from (using a distance threshold of 10 on the 100×100 grid as the definition of “close”). The burst origin was then computed as the mean of the remaining most active neurons’ x and y coordinates. These computed origins were manually examined to double-check that there were no unreasonable artifacts.

3.3. Overlapping Burst Identification

Bursts that originated near each other in time produced overlapping wavefronts that precluded further analysis for the purposes of this investigation. A simple method was implemented, similar to computation of burst wavefront described in section 3.4, to identify and exclude such overlapping bursts. In each

10ms window in each identified burst, those neurons that produced the most spikes were identified. For each member of that set of neurons, the distance to the origin was computed (note that, even if there were multiple overlapping bursts in the data, the method of section 3.2 only generated one origin). Then, for those windows that had at least three such distances, the standard deviation was compared to a threshold (a distance of 5.0 was used) and, if greater than that, the data for this “burst” was considered to include overlap from multiple bursts and excluded from further analysis. Because of the large number of bursts in the data, the threshold used was first tuned by hand and then spot-checked manually against a random 5% of bursts from all simulations to verify that overlapping bursts were filtered out without excluding isolated bursts.

3.4. Burst Propagation Speed

As bursts invariably originated at a single point and then propagated as wavefronts, the wavefront propagation speed was then determined for each burst to see if this changed during network development. This analysis was performed for each window from 100ms after burst start until 20ms before burst end. These were chosen to focus on windows where the most active neurons would lie on a substantial circular wavefront arc, rather than a central cluster or the burst’s “remnants” near the edge of the grid. For each window, those neurons that produced the most spikes were identified (these were invariably on the expanding wavefront), their distances to the origin were determined, the average distance was computed, and that value and the time from burst initiation was used to compute the propagation speed for that window. The computed speeds for each window making up a burst were then averaged to produce an average propagation speed for that burst. As the spatial grid used in the simulation is dimensionless, speed is presented in units of ms^{-1} .

3.5. Burst Origin Sequences

The temporal sequence of burst origins (x_i, y_i) , $1 \leq i \leq B$ (where B was the total number of non-overlapping bursts in a simulation), was then examined. These were first visualized by segmenting the entire simulation into 25 non-overlapping windows, to identify if origin spatial pattern changed during network development. For each window, the origins were plotted in the 2D plane with a line segment connecting each (x_i, y_i) with (x_{i+1}, y_{i+1}) to create *basic burst origin sequence* plots. Combining these plots together into a single 5×5 display created a simple visual representation of how burst origin patterns changed as network connectivity developed.

A variety of techniques were used to discern if the spatial sequence of burst origins within the network exhibited behavior that could be distinguished from random. Since the sequence pattern clearly changed as the network developed, this analysis was performed on the same 25 windows as above. Origin locations were categorized by dividing the 100×100 network into 10×10 tiles, corresponding to the simulation tiling pattern of excitatory, inhibitory, and endogenously active cells. Each origin was then assigned to the tile it fell within,

Table 1: Basic burst statistics for all four simulations.

| (ϵ, f) | Total Bursts | Overlapping Bursts |
|-----------------|--------------|--------------------|
| (1.9, 0.90) | 9,729 | 238 |
| (1.9, 0.98) | 9,160 | 126 |
| (1.0, 0.90) | 18,473 | 3,593 |
| (1.0, 0.98) | 17,659 | 844 |

so each (x_i, y_i) , $1 \leq x_i, y_i \leq 100$, was replaced with (x'_i, y'_i) , $1 \leq x'_i, y'_i \leq 10$; these were numbered sequentially as ℓ_i , $1 \leq \ell_i \leq 100$. The count of origins for each tile was used to visualize the frequency of origins for each tile. Since origins tended to cluster into a small number of tiles, only tiles that had non-zero origin counts were plotted as *burst origin histograms*. These histograms were tested against uniform distributions using a χ^2 test with $p < 0.05$ indicating non-uniform distributions.

These histograms were used to assess whether all origin clusters were equally likely. We also investigated sequential correlations between bursts by computing the joint frequencies of (ℓ_i, ℓ_{i+1}) , which we plotted as 5×5 displays of 2D images. As with simple histograms, only nonzero ℓ values were used in this analysis.

3.6. Burst Origins and Endogenously Active Neurons

All activity within these networks was driven by the endogenously active neurons; as described by Kawasaki and Stiber (2014), these were excitatory neurons with lowered spiking thresholds, thus capable of producing spikes solely due to their inherent noise currents. Each 10×10 tile established a regular pattern for the location of these neurons, which was done to avoid the inevitable spatial clustering that would have resulted if they were randomly distributed with independent probability. In these simulations, 10% of neurons (1000 out of the 10,000 total) were endogenously active. Each of these neurons was assigned a lowered threshold chosen randomly from a uniform distribution over a range that produced biologically realistic spiking rates.

The average spiking rate of an endogenously active neuron was therefore related to its lowered spiking threshold, and so the difference between this threshold and that of non-endogenously-active cells is a proxy for this average rate *in the absence of synaptic input*. We then related this location-based endogenous drive for the network with burst origin location by averaging the lowered thresholds of the endogenously active neurons within each 10×10 tile and plotting that as an image with the burst origins overlaid. We also computed Spearman's ρ and corresponding p for each simulation between number of origins in each tile and average threshold reduction for each tile.

4. Results

As mentioned in section 2.3, previous work had determined that sustained bursting with stationary neuronal outgrowth occurred for the four simulations

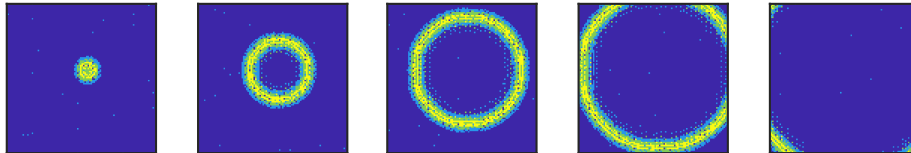


Figure 1: Example of a typical whole-network burst (chosen with origin near center of network for clarity). Each image includes 10ms of activity; lighter color corresponds to larger number of spikes by that particular neuron (dark blue corresponds to no spikes). Images are 30ms apart, starting 100ms after burst initiation.

whose results are presented below. In all four cases, during development neurons grew their radii of connectivity for a short time in which no bursts occurred; bursting began shortly after connections were formed between nearest neighbors. These bursts' statistics changed markedly as the simulations developed toward stationarity. Results in this paper are from analysis of all bursts from the four simulations $(\epsilon, f) = \{1.0, 1.9\} \times \{0.90, 0.98\}$, where ϵ is the outgrowth null point (firing rate at which a neuron's radius of connectivity would not change) and f was the fraction of the neurons that were excitatory (and thus $1 - f$ was the fraction that were inhibitory). Basic statistics are presented in table 1.

4.1. Burst Spatiotemporal Patterns

Figure 1 presents an example visualization of a typical whole network burst. Previous results indicated that bursts' durations and peak amplitudes changed markedly as network development progressed and that they originated at irregular time intervals that were indistinguishable from random (Kawasaki and Stiber, 2014). The spatiotemporal pattern results presented here invariably showed bursts originating at a single location and spreading as a wave of activity across the network. Occasionally, more than one burst would originate near the same time; these were excluded from further analysis as described in section 3.3; the number of those overlapping bursts is presented in table 1. The figure also shows the scattered, isolated spiking of endogenously active cells.

Given previous results' indication that bursts became briefer and more intense during network development, while still being composed of roughly the same number of spikes, and given these new results that from the start these bursts were waves of activity, we concluded that these developmental changes were likely due to increasing burst propagation speed. We analyzed burst wave propagation speed as a function of time during development as shown in figure 2. These graphs display propagation speed of individual bursts, along with a 100-burst moving average, versus burst number. Results are consistent with previous observations for all four bursting simulations in that faster wavefront propagation corresponds to briefer burst duration. The figure reveals a rapid increase in propagation speed early in development that levels out near simulation end (as the preparation's development becomes stationary). Speeds start around 0.2ms^{-1} (for $\epsilon = 1.9$) to 0.3ms^{-1} (for $\epsilon = 1.0$), meaning that it takes around 3.3–5.0ms to propagate from one neuron to a neighbor (horizontally or

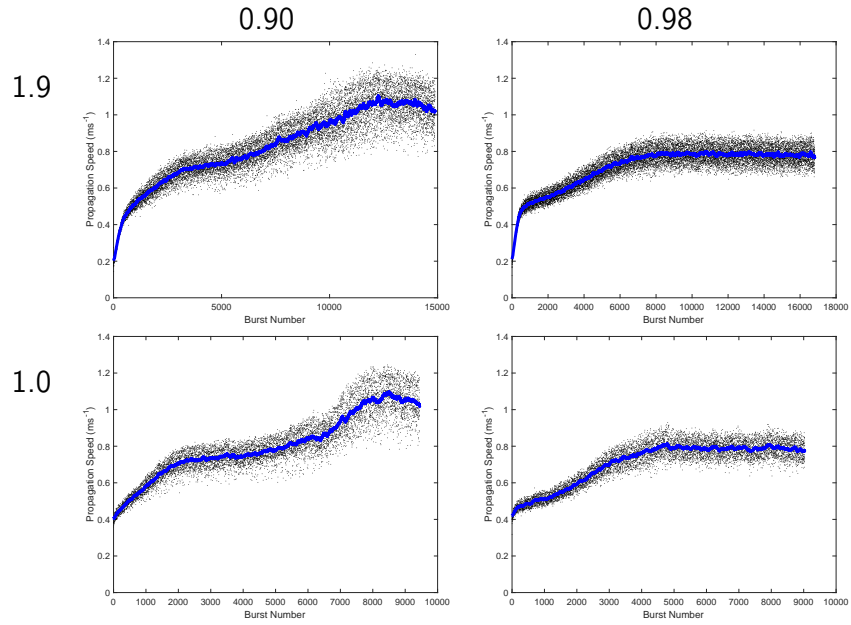


Figure 2: Burst speed during network development for individual bursts (points) and moving average of 100 bursts (bold line) and for given ϵ (indicated at left) and f (indicated above). While burst speed varies somewhat among bursts close in time, there is a clear trend.

Table 2: Spearman’s rank correlation computed to assess the relationship between burst speed and burst origin.

| (ϵ, f) | ρ | p |
|-----------------|--------|----------|
| (1.9, 0.90) | 0.037 | 0.000006 |
| (1.9, 0.98) | 0.11 | 0.0 |
| (1.0, 0.90) | -0.069 | 0.0 |
| (1.0, 0.98) | 0.017 | 0.116 |

vertically, since these simulations used rectangular connectivity; diagonal propagation would be $\sqrt{2}$ times greater). Speeds settle to around 0.4 (for $f = 0.98$) to 0.5ms^{-1} (for $f = 0.90$), or 2–2.5ms to propagate one neuron. This compares to synaptic transmission delays used in the simulation ranging from 0.8ms to 1.5ms.

Because there is a fair amount of variation in the individual bursts’ wave propagation speed during each stage of development, we tested the hypothesis that this is correlated with burst origin. This might be reasonable to expect, as the path of wavefront propagation depends on the origin location and different paths could correspond to sequences of synapses with different strengths. We tested this by converting burst origin 2D (x, y) indices to one dimension and computing Spearman’s rank correlation between burst speed and origin location, shown in table 2. One can see that there are negligible to very low, but

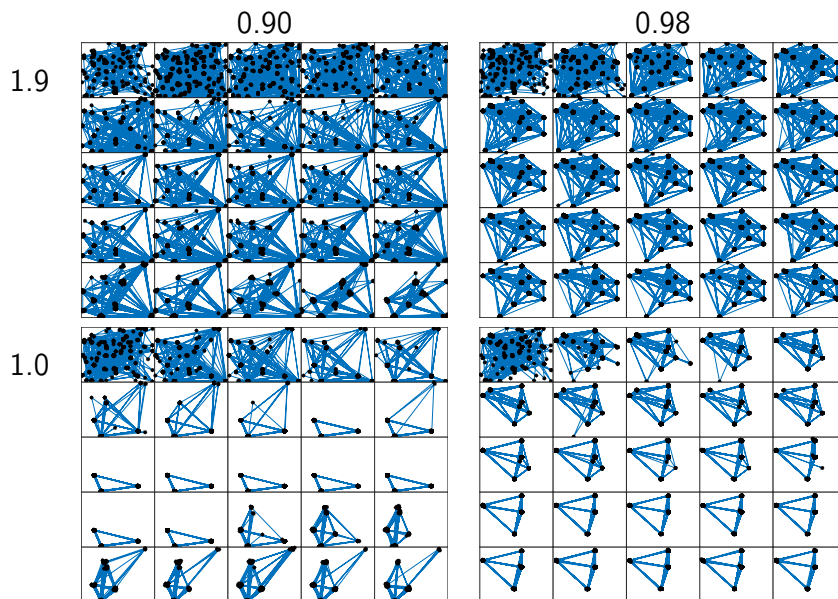


Figure 3: Basic burst origin sequence plots. Evolution of burst origins during development for given ϵ (indicated at left) and f (indicated above). Each of the 25 subgraphs in each plot displays sequential bursts in row-major order (i.e., with first block of bursts at top left and last block at bottom right). In each subgraph, burst origin locations are indicated within the 100×100 neuron culture by black asterisks (*) with each origin connected to the next with a blue line segment. Burst counts: $(\epsilon, f) = (1.9, 0.90)$: 14,880 origins, 596 origins/subgraph (576 for last subgraph); $(\epsilon, f) = (1.9, 0.98)$: 16,815 origins, 673 origins/subgraph (663 for last subgraph); $(\epsilon, f) = (1.0, 0.90)$: 9,446 origins, 378 origins/subgraph (374 for last subgraph); $(\epsilon, f) = (1.0, 0.98)$: 9,034 origins, 362 origins/subgraph (346 for last subgraph).

statistically significant, correlations for three of the simulations and a negligible, but not statistically significant, correlation for one. Thus, we have in some cases evidence for trivial (either not practically meaningful or of limited practical importance, given the large number of bursts) association between burst origin and speed and in one case no evidence for any association.

4.2. Burst Origins

Figure 3 displays the burst origin locations, sequences, and the evolution of sequence patterns during development for each of the four simulations. In all cases, origin locations tended to be more numerous early in development and later became restricted to a small subset; this is more pronounced for simulations with more inhibitory cells. These later sets of origin locations were stable over long durations — many thousands of bursts — though (as is particularly noticeable for the $\epsilon = 1.0$ Hz simulations) specific origins might disappear or appear over long periods of time.

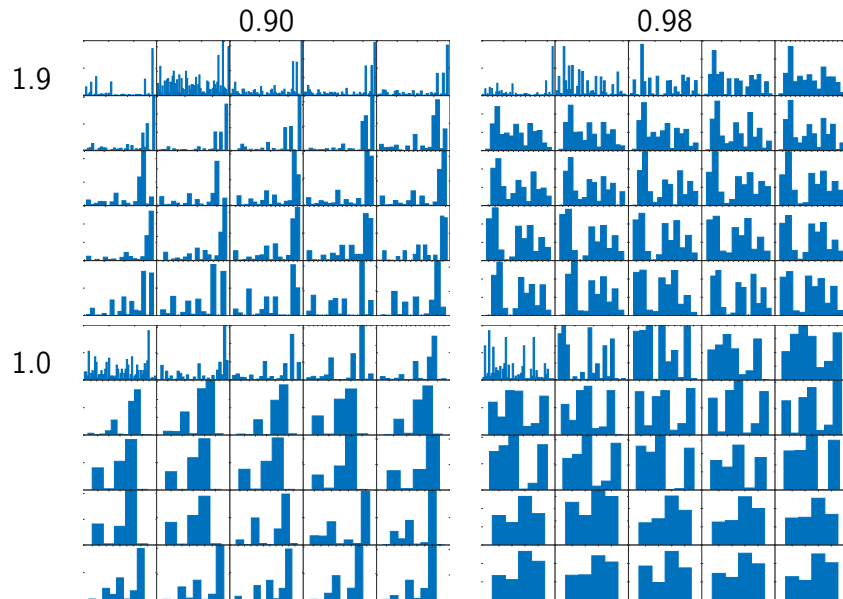


Figure 4: Burst origins histograms during development for given ϵ (indicated at left) and f (indicated above). Each of the 25 subgraphs in each plot displays histograms for the corresponding subgraph from figure 3. All histograms tested non-uniform.

4.3. Burst and Burst Sequence Probabilities

To the extent that burst origins were restricted to a small number of locations, figure 3 does not clearly show whether all locations were equally likely or if some were preferred. Figure 4 presents burst origin histograms for the four simulations and corresponding subgraphs. These clearly show the rapid reduction in number of regions in which bursts originate as development progressed. In almost all burst sequences, the distribution of bursts across the different origins was significantly non-uniform by χ^2 test ($p < 0.05$): some origins were more common, though even origins that were less common were generally not rare.

Figure 5 presents sequential correlations between each burst origin and the next for corresponding subgraphs, to test whether the origin of one burst was predictive of the next beyond their *a priori* frequency. As expected, bursts in the most common origin areas were most frequently succeeded by another burst in the same area. These joint histograms are approximately symmetric across the diagonal, with some of the asymmetry possibly resulting from the method used, which arbitrarily divided the network into fixed tiles. Thus, these results are consistent with the assertion that the sequence of burst origins was indistinguishable from random.

4.4. Burst Origins and Network Drive

We tested the cause of the non-uniformity of burst origin location by comparing it to the average network drive nearby. Figure 6 relates burst origins

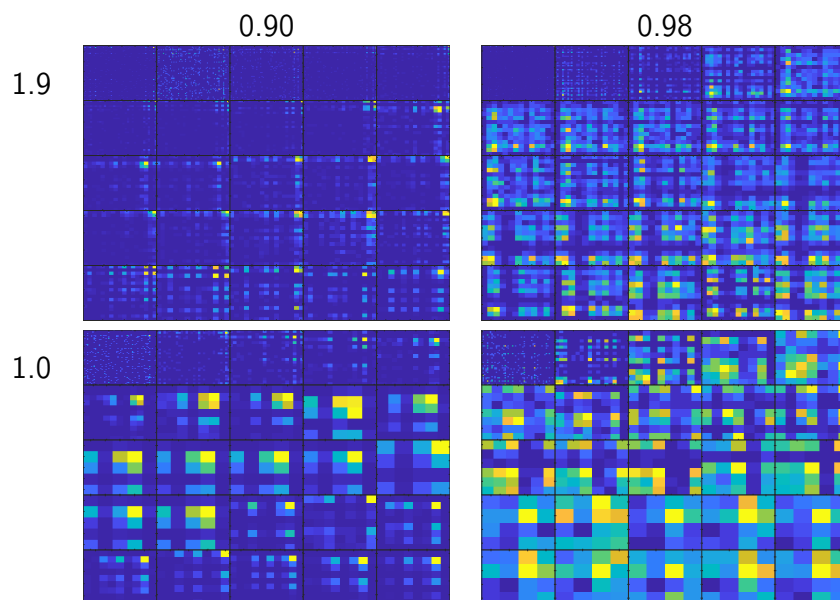


Figure 5: Sequential correlations for burst origins during development for given ϵ (indicated at left) and f (indicated above). Each of the 25 subgraphs in each plot displays (ℓ_i, ℓ_{i+1}) for the corresponding subgraph from figure 3.

Table 3: Spearman's rank correlation computed to assess the relationship between average threshold reduction in each 10×10 tile of neurons and number of burst origins in that tile.

| (ϵ, f) | ρ | p |
|-----------------|--------|-------|
| (1.9, 0.90) | -0.24 | 0.016 |
| (1.9, 0.98) | -0.31 | 0.002 |
| (1.0, 0.90) | -0.13 | 0.193 |
| (1.0, 0.98) | -0.25 | 0.010 |

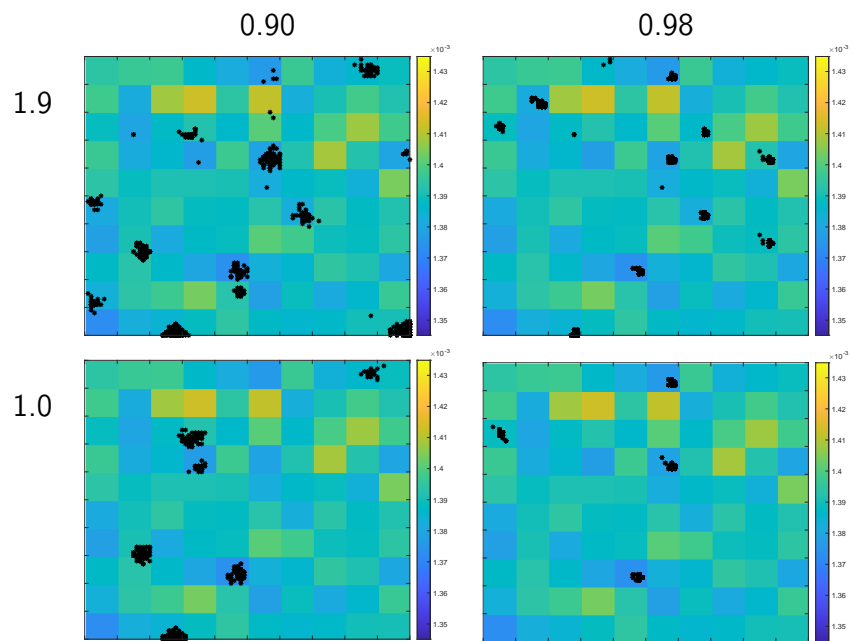


Figure 6: Plots of burst origins and average endogenously active neuron lowered threshold. Origins are for the bursts in the bottom row of the corresponding plots in figure 3. Each 10×10 tile of neurons in the network is represented by a color indicating the average amount that the 10 endogenously active neurons' threshold is lowered; more yellow indicates greater average lowered threshold and thus greater average spiking rate for those cells.

near the end of the simulations (when development became stationary) with the average amount that the 10 endogenously active neurons in each 10×10 tile of neurons had their spiking thresholds lowered. In the absence of synaptic input, a more greatly lowered threshold produces a higher average (noise driven) endogenous spiking rate. Thus, this is a measure of the average drive in that tile of neurons and the plots are a visual indication of whether bursts tend to originate in tiles with high levels of endogenous activity. By examination, burst origins are clearly not confined to the most active tiles. This was tested by computing Spearman’s rank correlation between burst count and lowered threshold for each tile, which is shown in table 3. One can see that there is a statistically significant, weak *negative* correlation between number of burst origins in a tile and network drive for that tile for three of the four simulations.

5. Discussion

This paper presented results from closed-loop simulations of neuron-activity-driven network development and the full spiking activity of all neurons in that developing network. This work used the simplest neuron/synapse models, and model of network development, that duplicated the salient features of *in vitro* burst development (Kawasaki and Stiber, 2014)—leaky integrators with synapses that include facilitation and resource depletion. We used this model to simulate development of networks from initially dissociated neurons and examined how spiking activity evolved along time towards stationarity. We also examined the dependence of that activity on two parameters: (1) the fraction of inhibitory neurons and (2) the average spiking rate at which neurite outgrowth/retraction was stable.

From these simulations, we can draw a number of conclusions, detailed in the following subsections, regarding the robustness of the bursting behavior, the nature of bursting as a network phenomenon, the spatiotemporal patterns of individual bursts, the evolution of individual bursts and burst origination as network connectivity changes, and the relationship between burst origination and local excitatory drive within the network.

5.1. *Burst development only requires a simple growth model; there is no need to fine tune model parameters*

We previously showed that bursting develops without the need to carefully select either the neuron or network growth model (only requiring that the activity of neurons affects that of other, connected, neurons and that such activity affects connectivity) and over a wide range of parameters (there is no need to precisely tune parameters to generate such whole-network bursts) (Kawasaki and Stiber, 2014). That work examined burst shape (defined in terms of overall network spiking rate) evolution during development and the statistics of inter-burst intervals. It is important to note that these are *network* bursts, as the neuron model used is not capable of endogenous bursting behavior. Previous work examined bursting solely in the time domain; the current work analyzes

spatio-temporal activity that includes every spike during one simulated month of development time.

It is instructive to compare the overall results here to that of Gritsun et al. (2012), who used much more detailed growth models, and greater cell type variety, in open-loop simulations in which neural activity did not affect development. Their spatiotemporal data had much coarser spatial resolution, as they were emulating experimental preparations that had 60 electrodes. They observed traveling waves (a type of activity common in neural dynamics (Ermentrout and Kleinfeld, 2001; Sato et al., 2012)), with “random” starting locations. They indicated that simulated bursts tended to start at network edges, due to boundary conditions (though one should note that there are also more neurons near the boundary than in the interior, and that alone could introduce a statistical bias towards network edges); detailed analysis of burst initiation spatial pattern was not done. Our findings are largely consistent with their major observations, without resort to complicated growth models or detailed and varied neuron models.

This lack of critical dependence on network or growth parameters is consistent with the speculation of Lonardoni et al. (2017) that such bursts naturally emerge during development under the condition of simple, distance-based constraints on connectivity. These constraints naturally apply to any network growth model that assumes that connection strength (density of synapses) is proportional to a density of neurites that decreases with distance from a cell body.

5.2. *Bursting is a network phenomenon*

As the individual neuron model used here is not capable of intrinsic bursting, the rapid firing of individual neurons as they contribute to wave propagation can only be a product of synaptic input from other neurons participating in the burst. The decline in spiking that produces a trailing edge for a wave must result from synaptic resources being exhausted. As a result, even in the case of multiple overlapping bursts, the wavefronts do not continue “through” each other like simple wave propagation, instead combining as they move through the neurons that have not yet participated in either burst.

This distinction between network bursting and intrinsic neural behavior can be seen in Figure 1, which not only shows a typical burst, but also reveals the low-level background spiking from endogenously active neurons before and after the wavefront passes by. This is possible because endogenous activity does not require synaptic input (and therefore no synaptic resources).

This is consistent with a broad theoretical literature relating to the general properties of networks of coupled oscillators (Ermentrout and Kleinfeld, 2001), and confirmation of the applicability of this theory in neural simulations (Sakuma et al., 2016; Senk et al., 2020), *in vitro* (Maeda et al., 1995), and *in vivo* (Sato et al., 2012; Okujeni et al., 2017; Muller et al., 2018; Davis et al., 2021). Our results seek to elicit the dependence of bursting characteristics on network development by looking at when during development bursting starts and how burst properties change as network connectivity changes. This builds

on previous results that bursts begin soon after connections form between neurons, that shortly thereafter connectivity patterns for excitatory and inhibitory neurons diverge, and that burst duration decreases as development progresses (Kawasaki and Stiber, 2014).

5.3. *Each burst originates at a single point and propagates as a wave of activity*

All of the bursts observed in simulations were like that shown in Figure 1, originating at single locations and propagating as traveling wavefronts across the network. Figures 2 and 3 illustrate how wavefront propagation speed and burst origin locations, respectively, evolved during network development. Such network wave propagation has frequently been suggested as underlying spatiotemporal network computation, such as in the visual system (Benigno et al., 2023).

On the other hand, we also see that a larger fraction of inhibitory cells (a five-fold difference here) produces faster-propagating bursts. This is consistent with broader connectivity among excitatory cells for smaller f (fraction of excitatory cells) (Kawasaki and Stiber, 2014, Figure 7).

5.4. *As development progresses, wave propagation speed increases*

Figure 2 shows that burst wavefront propagation speed increased during development (consistent with the findings of Maeda et al., 1995), by eye reaching stationarity by simulation end and corresponding to connectivity reaching stationarity in previous results (Kawasaki and Stiber, 2014). This increase in propagation speed explains previous simulation and experimental results (Van Pelt et al., 2004; vanPelt et al., 2004; Kawasaki and Stiber, 2014) that showed that early bursts start out with relatively long duration and low intensity, becoming briefer and more intense over time. Previous simulation data indicated the number of spikes produced did not vary much on average; the current results indicate that burst duration is a function of propagation speed: faster propagation corresponds to shorter burst duration. However, regardless of propagation speed, the width of the wavefront (duration of bursting by any single neuron) does not appear to change during development and, since bursts invariably propagate across the entire network, the total number of spikes within a burst is still constant.

It is also interesting that the initial and final propagation speeds appear to be most greatly influenced by different simulation parameters. In particular, initial propagation speed appears to depend on ϵ . This is the null point of the neurite outgrowth model; a higher value for ϵ means that connectivity change will continue until neurons are, on average (because outgrowth is several orders of magnitude slower than neuron spiking behavior), spiking almost twice as fast for the top row in the figure. From earlier results, this produced an extended period of time where average firing rate at first rapidly rose to around 1.0 and then more gradually continued to 1.9 (Kawasaki and Stiber, 2014, Figure 6). Those earliest bursts were significantly longer in duration for $\epsilon = 1.9$ (Figures 8 and 9 in Kawasaki and Stiber, 2014, around 800ms for $\epsilon = 1.9$ and 600ms for $\epsilon =$

1.0—these total propagation times are consistent with the propagation speeds observed here). Moreover, this occurred earlier during development for larger ϵ (Kawasaki and Stiber, 2014, Figure 9), consistent with the higher derivative from equation 7.

The most obvious difference produced by increased ϵ was seen in more frequent bursting (Kawasaki and Stiber, 2014, Figure 11), both early on and throughout the simulation (which is consistent with the burst numbers seen in table 1 and Figure 2 here). This makes sense because the number of spikes each neuron contributes to a burst is largely governed by synaptic resources, as discussed previously, so a greater average spiking rate must result from more frequent burst production. Our conclusion is that this translates into earlier connectivity producing a larger number of longer-duration bursts, slower-propagating at first, with connectivity more rapidly growing leading to a more rapid increase in burst propagation speed.

On the other hand, final propagation speeds appear to depend on f , the fraction of excitatory cells (a five-fold difference in inhibitory cells here): more inhibition results in more rapidly propagating waves. This is consistent with broader connectivity among excitatory cells for smaller f (Kawasaki and Stiber, 2014, Figure 7).

A fair amount of variation is seen in the propagation speed computed for individual bursts at about the same stage in development. Due to the lack of substantive correlation between propagation speed and burst origin (table 2), we hypothesize that this could be ascribed to the analysis algorithm, which only used the most active cells for each 10ms of a burst.

5.5. *Early in development, bursts originate at many locations; later, bursts originate at only a few*

Our results show that bursts propagate as waves that originate from compact points in the network, or “origins”. These origins correspond to what have been identified *in vitro* as functional communities (fCOMs, Lonardoni et al., 2017) or, in terms in individual cells that participate earliest in burst initiation, major burst leaders (MBLs, Pasquale et al., 2013). While our simulations provide much greater spatiotemporal resolution than cortical cultures on multi-electrode arrays, our work here does not seek to distinguish between burst initiation by cell communities versus individual cells (or even if such a distinction is meaningful in the context of neural networks). However, it is important to point out that these are not incompatible views, as fCOMs must be composed of individual MBL cells.

What is clear is that early in development there are many burst origin locations and that the number of origin locations in the network decreases until stationarity (Figure 3). We suggest that this is consistent with the fact that network connectivity is maximally localized early on (beginning when neurons are only 4-connected in these simulations) and becomes broader as development progresses (though connectivity is still localized, as the final radii of neurite outgrowth for all neurons are not much greater than 2, see Kawasaki and Stiber

(2014, Figure 7)). Moreover, the overall reduction of origins during development occurs without cell death or connection pruning. These results demonstrate that, while these networks are large and complex enough to support burst initiation virtually anywhere, even relatively localized connectivity can restrict initiation to a bare handful of fCOMs (or, alternatively, to a small subset of neurons as MBLs).

We can also see in Figures 3 and 4 that, while these results hold over a range of (ϵ, f) , these parameters are influential in the evolution toward fCOMs/MBLs. A higher target firing rate produces more bursts (roughly 15,000–18,000 for $\epsilon = 1.9$ versus around 10,000 for $\epsilon = 1.0$) and more origins. On the other hand, a greater fraction of inhibitory neurons (smaller f) produces slower evolution towards the final set of origins.

5.6. The origin of each burst is independent of others

Given that bursts originate at only certain locations at any given time during development, one might ask whether these locations were all equally preferred and if the aftereffects of a burst originating at one location might affect the probability of the next burst originating at other locations. This wouldn't necessarily require direct connectivity among fCOMs/MBLs; it might be the result of different pathways followed by bursting wavefronts at each.

Our results show that not all burst origins were equally likely, as all of the histograms of number of bursts at each origin during development were significantly non-uniform (Figure 3). Sequential correlations (Figure 5) were indistinguishable by the methods used from random. Thus, we conclude that the origin point for any individual burst does not appear to depend on that of preceding bursts. This is understandable given the relatively long duration between bursts compared to any simulation state variable's time constant (Kawasaki and Stiber, 2014).

5.7. Burst origination seems to be a network phenomenon

A central question of bursting is why certain locations correspond to fCOMs/MBLs while others don't. This is closely connected to the question of what triggers a burst. This question is particularly salient late in development when connectivity is stationary and only a very small handful of locations among the 10,000 neurons in the network are burst origins. A reasonable hypothesis regarding why bursts start at particular locations in the network would be that those are the regions with the largest drive from the endogenously active neurons. After all, since there is no external input in these simulations, it is only by virtue of those neurons' activities that any spiking occurs at all in these networks. However, if that were the case, then Figure 6 would be expected to show that the most common origin locations corresponded to those tiles of neurons with the most active neurons and that is clearly not so, verified in table 3. Thus, not only can we say that the bursting itself is an emergent behavior from the network during development (since these neuron models are not capable of endogenous bursting), but burst initiation itself, and therefore the existence of fCOMs/MBLs, is an emergent property.

6. Future Work

This paper establishes a number of activities of developing neural networks that emerge from the network, rather than the individual neurons. However, particularly given the localized nature of many of the events described here (such as burst initiation), their true interpretation must lie at the mesoscale. In particular, the existence of a small number of origin locations in the face of a lack of correlation with network drive implies that local connectivity patterns, or motifs, must dictate fCOMs/MBLs. The question remains regarding what those motifs might be.

Burst also originate at particular points in time. Our results have demonstrated that neurons and synapses recover from the aftereffects of a burst and then some variable and significant amount of time passes before the next. In other words, a burst is not produced just as soon as the network (or the existing fCOMs/MBLs) is capable. So, it must be the case that there is some pattern of triggering activity that kicks off a burst, and this pattern is somewhat uncommon. What is that pattern and in what way does it differ from patterns that don't trigger bursts? How do such patterns interact with or are shaped by fCOM/MBL motifs?

We must also recognize that the neurite outgrowth and network formation simulated here represents just one phase of biological neural network development. Subsequent to this first stage of synaptogenesis, where connections are over-produced, comes a refinement stage where mechanisms such as spike timing dependent plasticity (STDP) strengthen, weaken, and prune synapses. Just as we ask questions about the interplay of neuron (microscale), motif (mesoscale), and network (macroscale) for bursting here, STDP simulation would allow us to examine how network architectures and behaviors change as connectivity is tuned—both endogenously from the bursts themselves and due to functional considerations in the presence of external inputs, outputs, and feedback.

7. Acknowledgments

The authors thank Fumitaka Kawasaki, Navee Kaur, Kate Sprague, and Tom Wong for their helpful discussions and software development work. MS thanks the Fulbright program of the US Dept. of State and the Czech Republic Fulbright Commission for their support and the Institute of Physiology of the Czech Academy of Sciences for their hospitality and discussions related to this work.

References

- Abbott, L., 1999. Lapicque's introduction of the integrate-and-fire model neuron (1907). *Brain Research Bulletin* 50, 303–304. URL: <https://linkinghub.elsevier.com/retrieve/pii/S0361923099001616>, doi:10.1016/S0361-9230(99)00161-6.

- Benigno, G.B., Budzinski, R.C., Davis, Z.W., Reynolds, J.H., Muller, L., 2023. Waves traveling over a map of visual space can ignite short-term predictions of sensory input. *Nature Communications* 14, 3409. URL: <https://www.nature.com/articles/s41467-023-39076-2>, doi:10.1038/s41467-023-39076-2.
- Davis, Z.W., Benigno, G.B., Fletteman, C., Desbordes, T., Steward, C., Sejnowski, T.J., H. Reynolds, J., Muller, L., 2021. Spontaneous traveling waves naturally emerge from horizontal fiber time delays and travel through locally asynchronous-irregular states. *Nature Communications* 12, 6057. URL: <https://www.nature.com/articles/s41467-021-26175-1>, doi:10.1038/s41467-021-26175-1.
- Davis, Z.W., Muller, L., Martinez-Trujillo, J., Sejnowski, T., Reynolds, J.H., 2020. Spontaneous travelling cortical waves gate perception in behaving primates. *Nature* 587, 432–436. URL: <https://www.nature.com/articles/s41586-020-2802-y>, doi:10.1038/s41586-020-2802-y.
- Eckmann, J.P., Jacobi, S., Marom, S., Moses, E., Zbinden, C., 2008. Leader neurons in population bursts of 2D living neural networks. *New Journal of Physics* 10, 015011. URL: <https://iopscience.iop.org/article/10.1088/1367-2630/10/1/015011>, doi:10.1088/1367-2630/10/1/015011.
- Ermentrout, G.B., Kleinfeld, D., 2001. Traveling Electrical Waves in Cortex: Insights from Phase Dynamics and Speculation on a Computational Role. *Neuron* 29, 33–44.
- Eytan, D., Marom, S., 2006. Dynamics and Effective Topology Underlying Synchronization in Networks of Cortical Neurons. *The Journal of Neuroscience* 26, 8465–8476. URL: <https://www.jneurosci.org/lookup/doi/10.1523/JNEUROSCI.1627-06.2006>, doi:10.1523/JNEUROSCI.1627-06.2006.
- Gritsun, T.A., Le Feber, J., Rutten, W.L.C., 2012. Growth Dynamics Explain the Development of Spatiotemporal Burst Activity of Young Cultured Neuronal Networks in Detail. *PLoS ONE* 7, e43352. URL: <https://dx.plos.org/10.1371/journal.pone.0043352>, doi:10.1371/journal.pone.0043352.
- Gross, G.W., 1979. Simultaneous single unit recording in vitro with a photoetched laser deinsulated gold multielectrode surface. *IEEE Transactions on Biomedical Engineering* 26, 273–9.
- Huang, C.H., Huang, Y.T., Chen, C.C., Chan, C.K., 2017. Propagation and synchronization of reverberatory bursts in developing cultured networks. *Journal of Computational Neuroscience* 42, 177–185. URL: <http://link.springer.com/10.1007/s10827-016-0634-4>, doi:10.1007/s10827-016-0634-4.

- Kawasaki, F., Stiber, M., 2012. Bursting behavior in a large-scale model of cortical network development, in: *BIOCOMP 2012 — Mathematical Modeling and Computational Topics in Biosciences*.
- Kawasaki, F., Stiber, M., 2014. A simple model of cortical culture growth: burst property dependence on network composition and activity. *Biological Cybernetics* 108, 423–443. URL: <http://link.springer.com/10.1007/s00422-014-0611-9>, doi:10.1007/s00422-014-0611-9.
- Klavinskis-Whiting, S., Bitzenhofer, S., Hanganu-Opatz, I., Ellender, T., 2023. Generation and propagation of bursts of activity in the developing basal ganglia. *Cerebral Cortex* 33, 10595–10613. URL: <https://academic.oup.com/cercor/article/33/20/10595/7248982>, doi:10.1093/cercor/bhad307.
- Lonardoni, D., Amin, H., Di Marco, S., Maccione, A., Berdoncini, L., Nieuwenhuis, T., 2017. Recurrently connected and localized neuronal communities initiate coordinated spontaneous activity in neuronal networks. *PLOS Computational Biology* 13, e1005672. URL: <https://dx.plos.org/10.1371/journal.pcbi.1005672>, doi:10.1371/journal.pcbi.1005672.
- Maeda, E., Robinson, H., Kawana, A., 1995. The mechanisms of generation and propagation of synchronized bursting in developing networks of cortical neurons. *The Journal of Neuroscience* 15, 6834–6845. URL: <https://www.jneurosci.org/lookup/doi/10.1523/JNEUROSCI.15-10-06834.1995>, doi:10.1523/JNEUROSCI.15-10-06834.1995.
- Markram, H., Wang, Y., Tsodyks, M., 1998. Differential signaling via the same axon of neocortical pyramidal neurons. *Proc. Natl. Acad. Sci. USA* 95, 5323–8.
- Muller, L., Chavane, F., Reynolds, J., Sejnowski, T.J., 2018. Cortical travelling waves: mechanisms and computational principles. *Nature Reviews Neuroscience* 19, 255–268. URL: <https://www.nature.com/articles/nrn.2018.20>, doi:10.1038/nrn.2018.20.
- Okujeni, S., Kandler, S., Egert, U., 2017. Mesoscale Architecture Shapes Initiation and Richness of Spontaneous Network Activity. *The Journal of Neuroscience* 37, 3972–3987. URL: <https://www.jneurosci.org/lookup/doi/10.1523/JNEUROSCI.2552-16.2017>, doi:10.1523/JNEUROSCI.2552-16.2017.
- Paraskevov, A.V., Zendrikov, D.K., 2017. A spatially resolved network spike in model neuronal cultures reveals nucleation centers, circular traveling waves and drifting spiral waves. *Physical Biology* 14, 026003. URL: <https://iopscience.iop.org/article/10.1088/1478-3975/aa5fc3>, doi:10.1088/1478-3975/aa5fc3.

- Pasquale, V., Martinoia, S., Chiappalone, M., 2013. Leader neurons drive spontaneous and evoked activation patterns in cortical networks. *BMC Neuroscience* 14, P64, 1471–2202–14–S1–P64. URL: <https://bmcneurosci.biomedcentral.com/articles/10.1186/1471-2202-14-S1-P64>, doi:10.1186/1471-2202-14-S1-P64.
- Pasquale, V., Martinoia, S., Chiappalone, M., 2017. Stimulation triggers endogenous activity patterns in cultured cortical networks. *Scientific Reports* 7, 9080. URL: <https://www.nature.com/articles/s41598-017-08369-0>, doi:10.1038/s41598-017-08369-0.
- Pine, J., 1980. Recording action potentials from cultured neurons with extracellular microcircuit electrodes. *jnm* 2, 19–31.
- Sakuma, S., Mizuno-Matsumoto, Y., Nishitani, Y., Tamura, S., 1 Graduate School of Applied Informatics, University of Hyogo, Kobe 650-0047, Japan;, 2016. Simulation of Spike Wave Propagation and Two-to-one Communication with Dynamic Time Warping. *AIMS Neuroscience* 3, 474–486. URL: <http://www.aimspress.com/article/10.3934/Neuroscience.2016.4.474>, doi:10.3934/Neuroscience.2016.4.474.
- Sato, T., Nauhaus, I., Carandini, M., 2012. Traveling Waves in Visual Cortex. *Neuron* 75, 218–229. URL: <https://linkinghub.elsevier.com/retrieve/pii/S0896627312005910>, doi:10.1016/j.neuron.2012.06.029.
- Senk, J., Korvasová, K., Schuecker, J., Hagen, E., Tetzlaff, T., Diesmann, M., Helias, M., 2020. Conditions for wave trains in spiking neural networks. *Physical Review Research* 2, 023174. URL: <https://link.aps.org/doi/10.1103/PhysRevResearch.2.023174>, doi:10.1103/PhysRevResearch.2.023174.
- Stegenga, J., Le Feber, J., Marani, E., Rutten, W., 2008. Analysis of Cultured Neuronal Networks Using Intraburst Firing Characteristics. *IEEE Transactions on Biomedical Engineering* 55, 1382–1390. URL: <http://ieeexplore.ieee.org/document/4400839/>, doi:10.1109/TBME.2007.913987.
- Stiber, M., Kawasaki, F., Davis, D.B., Asuncion, H.U., Lee, J.Y.H., Boyer, D., 2017. BrainGrid+Workbench: High-performance/high-quality neural simulation, in: 2017 International Joint Conference on Neural Networks (IJCNN), IEEE, Anchorage, AK, USA. pp. 2469–2476. URL: <http://ieeexplore.ieee.org/document/7966156/>, doi:10.1109/IJCNN.2017.7966156.
- Stiber, M., Kawasaki, F., Wong, T., Lee, J., Davis, D., Conrad, A., Oziel, A., McLean, D., 2018. UWB-Biocomputing/BrainGrid: Release for spring 2018. URL: <https://doi.org/10.5281/zenodo.1200192>, doi:10.5281/zenodo.1200192.

- Stiber, M., O’Keefe, Christopher, Martinez, J., Elgazzar, O., Kamath, D., Salvatore, T., Madison, A., Rudrawar, A., Neary, A., Brown, J., Gandhi, V., Sorvik, M., Andrzej-Dawiec, Hsu, C., Arndorfer, V., Pal, P., Dukart, K., Li, X., Saini, J.K., Posey, N., McIntosh, C., Shaikh, Z., 2025a. UWB-Biocomputing/Graphitti: Let the git flow. URL: <https://doi.org/10.5281/zenodo.15257819>, doi:10.5281/zenodo.15257819.
- Stiber, M., Taneja, A., Scott, L., Singh, S., Arndorfer, V., Gonzales, N., Martinez, J., Hsu, E., Singh, S., Lundvall, M., 2025b. UWB-Biocomputing/GraphSystemsAnalysis: It’s about time. URL: <https://doi.org/10.5281/zenodo.17100930>, doi:10.5281/zenodo.17100930.
- Thomas, Jr., C., Springer, P., Loeb, G., Berwaldnetter, Y., Okun, L., 1972. A miniature microelectrode array to monitor the bioelectric activity of cultured cells. *Experimental Cell Research* 74, 61–66. URL: <https://linkinghub.elsevier.com/retrieve/pii/0014482772904818>, doi:10.1016/0014-4827(72)90481-8.
- Tsodyks, M., Pawelzik, K., Markram, H., 1998. Neural networks with dynamic synapses. *Neural Computation* 10, 821–35.
- Van Ooyen, A., Van Pelt, J., 1996. Complex Periodic Behaviour in a Neural Network Model with Activity-Dependent Neurite Outgrowth. *Journal of Theoretical Biology* 179, 229–242. URL: <https://linkinghub.elsevier.com/retrieve/pii/S0022519396900636>, doi:10.1006/jtbi.1996.0063.
- Van Ooyen, A., Van Pelt, J., Corner, M., 1995. Implications of activity dependent neurite outgrowth for neuronal morphology and network development. *Journal of Theoretical Biology* 172, 63–82. URL: <https://linkinghub.elsevier.com/retrieve/pii/S0022519385700057>, doi:10.1006/jtbi.1995.0005.
- Van Pelt, J., Corner, M., Wolters, P., Rutten, W., Ramakers, G., 2004. Longterm stability and developmental changes in spontaneous network burst firing patterns in dissociated rat cerebral cortex cell cultures on multielectrode arrays. *Neuroscience Letters* 361, 86–89. URL: <https://linkinghub.elsevier.com/retrieve/pii/S0304394003015283>, doi:10.1016/j.neulet.2003.12.062.
- vanPelt, J., Wolters, P., Corner, M., Rutten, W., Ramakers, G., 2004. Long-Term Characterization of Firing Dynamics of Spontaneous Bursts in Cultured Neural Networks. *IEEE Transactions on Biomedical Engineering* 51, 2051–2062. URL: <http://ieeexplore.ieee.org/document/1344208/>, doi:10.1109/TBME.2004.827936.

Zbinden, C., 2011. Leader neurons in leaky integrate and fire neural network simulations. *Journal of Computational Neuroscience* 31, 285–304. URL: <http://link.springer.com/10.1007/s10827-010-0308-6>, doi:10.1007/s10827-010-0308-6.